

Enhanced photocatalytic degradation of organic pollutants using Zn-Doped TiO₂ nanoparticles synthesized via a novel hydrothermal method

X. G. Chen ^{a,d,#}, J. T. Shuai ^{a,d,#}, Y. J. Chen ^{a,d}, L. J. Wang ^b, X. N. Chi ^c,
D. W. Zhang ^d, H. J. Song ^{a,d}, J. Q. Chen ^{a,d,*}

^a School of Mechanical Engineering, Chengdu University, Chengdu, 610106, China

^b School of New Materials and Chemical Engineering, Guang'an Vocational & Technical College, Guang'an, 638000, China

^c China Center for Information Industry Development, CCID Industrial and Information Technology Research Institute (Group) Sichuan Co, Ltd, Chengdu 610200, China

^d Sichuan Province Engineering Research Center for Powder Metallurgy, Chengdu University, Chengdu 610106, China

^e Sichuan Aerospace Chuannan Initiating Explosive Technology Limited, Luzhou 646000, China

Transition metal doping, including Zn, is a promising method among various doping strategies employed to enhance TiO₂ photocatalysts. However, several challenges such as non-uniform distribution of Zn ions, particle agglomeration, poor stability still exist. To address these limitations, this study presents the development of Zn-doped TiO₂ (Zn-TiO₂) nanoparticles via a novel hydrothermal synthesis method utilizing oxalic acid (OA) as a hydrolysis inhibitor and also a capping agent. This innovative approach ensures uniform Zn doping and formation of a unique nano-flower-like morphology, significantly enhancing the photocatalytic properties. The Zn-TiO₂ catalysts demonstrated remarkable photodegradation efficiency, under simulated light at 100 mW/cm², methyl orange achieved complete degradation within thirty minutes. This improved performance is due to the significantly increased surface area, enhancing the retention of photogenerated charge carriers by minimizing their recombination rate, while also broadening the spectral range of light absorption to encompass the visible spectrum. Furthermore, the catalysts exhibit excellent stability and recyclability, maintaining high activity over multiple cycles. Mechanistic investigations indicate that superoxide radicals (O²⁻) and holes (h⁺) are essential in boosting photocatalytic activity. The results offer important insights for the design of advanced photocatalysts and underscore the importance of doping strategies in enhancing the functional properties of TiO₂ for practical applications in environmental technology.

(Received December 24, 2024; Accepted April 1, 2025)

Keywords: Zn-TiO₂, Doping, Photocatalysis, Degradation, Nano-flower

These authors contributed equally to the work and should be regarded as co-first authors.

* Corresponding authors: chenjiaqi@cdu.edu.cn

<https://doi.org/10.15251/DJNB.2025.202.383>

1. Introduction

The study of photocatalytic degradation of organic contaminants has emerged as a vital field of investigation in response to the escalating requirement for pristine water sources and the imperative to alleviate environmental contamination. In recent years, semiconductor materials have shown vast potential in wastewater treatment. The application of various semiconductor nanoparticles in the photocatalytic degradation of different water pollutants under visible light, sunlight, and UV radiation has emerged as a focal point of research. In standard photocatalytic processes, electrons are elevated from the valence band (VB) to the conduction band (CB), resulting in the creation of a vacancy in the VB, triggered by photons whose energy equals or greater than the semiconductor band gap [1]. These photogenerated electrons and holes are primarily responsible for various photocatalytic activities [2-4]. Common semiconductor photocatalysts include ZnO [5, 6], TiO₂ [7, 8], Fe₂O₃ [9, 10], CuS [11, 12], ZnS [13, 14], WO₃ [15, 16], and SnO₂ [17, 18], typically characterized as n-type semiconductors with a discontinuous band structure distinct from metals, usually composed of filled electron-rich lower energy bands. Among these [19], TiO₂ remains a cornerstone in semiconductor photocatalysis for water treatment, owing to its longstanding research history and inherent benefits: chemical stability, minimal toxicity, abundance, cost-effectiveness, and ease of synthesis [20, 21].

However, as a typical photocatalyst, pure TiO₂ has significant drawbacks when used in pollution treatment, namely, its wide band gap and narrow light absorption range [22, 23]. Moreover, poor charge carrier mobility results in a significant rate of recombination between electron-hole pairs [24]. To address these limitations, various modification strategies, including doping with transition metals and utilizing organic ligands [25], have been explored extensively. Among these, the doping of Zn into TiO₂ results in increased photocatalytic performance [26-28] by narrowing the bandgap [29, 30], thereby extending light absorption into the visible region and improving charge separation efficiency [31, 32]. Despite these potential benefits, several challenges persist with existing Zn-TiO₂ materials. For instance, traditional doping methods such as sol-gel and mechanical mixing often result in non-uniform distribution of Zn ions [33], poor crystallinity [34], and particle agglomeration [35, 36], which negatively impact the photocatalytic activity. Additionally, many Zn-TiO₂ nanoparticles suffer from instability and limited recyclability, further constraining their practical use [37, 38].

To overcome these challenges, our study presents a novel hydrothermal synthesis method to produce uniformly Zn-TiO₂ nanoparticles. This method incorporates oxalic acid (OA) as a hydrolysis inhibitor and capping agent [39], which serves a dual function in controlling the growth of nanostructures and ensuring homogeneous Zn doping. The capability of these materials as catalysts to degrade methyl orange (MO) dye was evaluated. Characterization techniques, such as XRD, SEM, TEM, PL, and UV-Vis DRS were used to analyze their properties. Order to improve the optical absorption capacity of TiO₂ across the UV-vis spectrum, the photocatalytic activities of zinc-doped TiO₂, using zinc as transition metal were investigated. These techniques reveal that the Zn-TiO₂ nanoparticles possess a significantly larger surface area compared to those synthesized by conventional methods. The unique nano-flower-like morphology further contributes to the superior photocatalytic performance by augmenting the availability of reactive surfaces for the breakdown of organic contaminants.

2. Methods

2.1. Materials

Zinc nitrate hexahydrate ($\text{Zn}(\text{NO}_3)_2 \cdot 6\text{H}_2\text{O}$, CAS: 10196-18-6, 99%) was obtained from Chengdu Kolon Chemical Co, Ltd. benzoquinone (BQ, CAS: 106-51-4, 97%), Ammonium oxalate (AO, CAS: 1113-38-8, 98%) and tert-butanol (TBA, CAS: 75-65-0, 99%) were purchased from Ron Chemicals. Tetra-n-butyl orthotitanate (TBOT, CAS: 5593-70-4, 98%), oxalic acid (OA, CAS: 144-62-7, 99%), ethanol (CAS: 64-17-5, 99.5%) and methyl orange (MO, CAS: 547-58-0, 96%) were provided by Aladdin Chemicals, Shanghai, China.

2.2. Synthesis of Zn-TiO₂

90 mL of anhydrous ethanol was measured and added to a three-necked flask. Under vigorous stirring at room temperature, 10 mL of tetra-n-butyl orthotitanate (TBOT) was added, followed by thorough mixing with 2.505 g of OA for 10 minutes until the solution turned uniformly milky, forming solution A. To prepare solution B, 10 mL of deionized water was mixed with 0.438 g of zinc nitrate hexahydrate ($\text{Zn}(\text{NO}_3)_2 \cdot 6\text{H}_2\text{O}$). Solution B was then gradually added dropwise to solution A, while stirring continuously for 5 hours. The resulting mixture was dried at 60°C and calcined at 500°C for 2 hours to obtain Zn-TiO₂.

2.3. The photocatalytic degradation properties of MO

In this study, a 300 W xenon lamp (CME-Xe300F/UV) was used as the light source with an AM1.5 filter to simulate solar light (100 mW/cm²). A quantity of 0.1 grams of either TiO₂ or Zn-TiO₂ photocatalyst was suspended within a 20 ml aqueous solution containing MO at a concentration of 20 mg/L. This mixture was agitated without exposure to light for roughly 30 minutes to achieve equilibrium in the adsorption-desorption process between the photocatalyst and the dye molecules. Then, the solution was exposed to irradiated with full spectrum UV-vis light from the 300 W xenon lamp. Stirring was maintained during irradiation to keep the suspension homogeneous. Every 10 minutes, a sample of the suspension was subjected to centrifugation, with the resulting supernatant being retrieved and marked. The remaining concentration of the MO dye was ascertained by examining the solution's absorbance at varying time points with a UV-visible spectrophotometer (UV-2800A), under UV-vis spectroscopy. Changes in the UV-visible absorption spectra showed a peak absorption of MO at $\lambda_{\text{max}} = 465$ nm. The gradual color change of the MO dye to colorless indicated the oxidation of the MO dye.

3. Results and discussion

3.1. SEM analysis

SEM is a commonly used characterization method for depicting the morphology and microstructure of catalysts. As shown in Fig. 1, particles of different photocatalysts exhibit varying shapes and sizes. SEM images (Fig. 1a, b) of TiO₂ reveal locally aggregated blocky structures with rough surfaces (Fig. 1a).

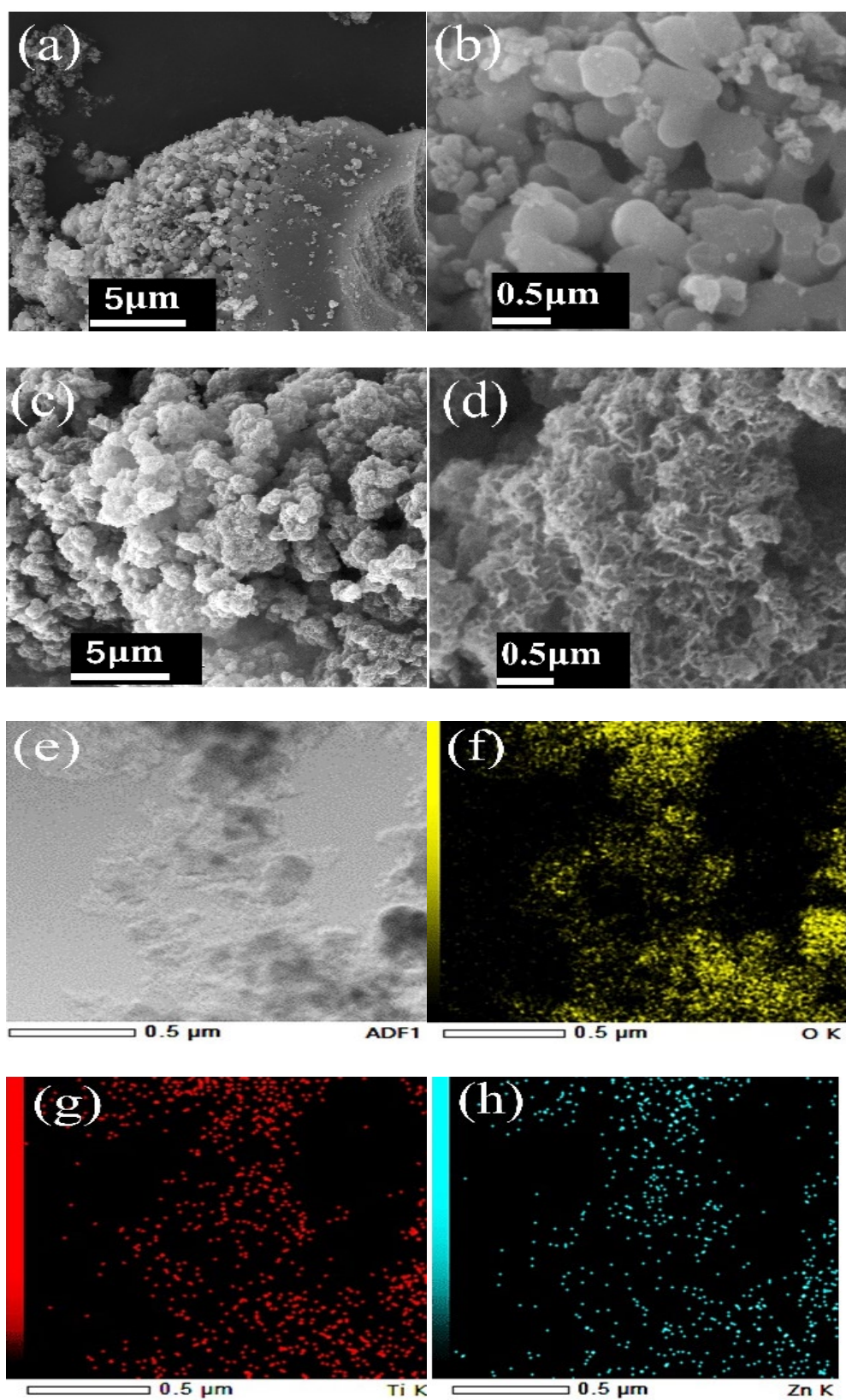


Fig. 1. Morphology of nanocatalysts. SEM images of (a, b) TiO_2 , and (c, d) Zn-TiO_2 . (e) the HAADF-STEM image of Zn-TiO_2 , along with elemental distribution maps of (f) O, (g) Ti and (h) Zn.

Upon closer inspection, these structures consist of irregularly aggregated particles with smooth surfaces, demonstrating a broad range of dimensions, the particles exhibited an average diameter of $0.38 \pm 0.01 \mu\text{m}$ (Fig. 1b, S1a). The Zn doping results in a more rugged coral-like surface (Fig. 1c). Further magnification reveals a nano-flower-like morphology with particles averaging $27.38 \pm 0.31 \text{ nm}$ (Fig. 1d, S1b). The TEM image (Fig. S2) also reveals morphology features consistent with SEM observations. We also obtained the elemental mapping of Zn-TiO₂ (Fig. 1e-h), which demonstrates that the catalyst is primarily composed of Ti, Zn, and O with all uniform distributions. Thus, the use of OA ensures uniform Zn doping and prevents particle agglomeration, resulting in a unique nano-flower-like morphology, implying significantly increased surface area and active sites conducive to enhancing photocatalytic performance.

3.2. X-ray diffraction analysis

XRD is a commonly used method for characterizing material crystal structures, which is crucial for the study of photocatalysts. The XRD results of photocatalysts reveal a series of sharp diffraction peaks (Fig. 2), where each peak's position and intensity correspond to specific interplanar spacings and crystal lattice arrangements. Powder XRD patterns were studied for pure TiO₂ and Zn-TiO₂ within the 2θ range of 10° to 80° . Regarding TiO₂, the peaks observed in the diffraction spectrum at 25.3° , 37.8° , 48.0° , 53.9° , 55.1° , and 62.7° are attributed to the (101), (004), (200), (105), (211), and (204) lattice planes, suggesting the occurrence of rutile phase in the TiO₂ sample. The XRD spectra of the catalysts predominantly exhibit reflections characteristic of rutile TiO₂ structure. Additionally, a peak at 27.4° corresponding to the (110) crystal plane suggests the existence of an anatase phase of TiO₂. The peaks of TiO₂ are sharper and indicate higher purity, whereas for Zn-TiO₂, with increasing Zn content, the crystallinity of TiO₂ decreases. This suggests that the incorporation of Zn into the TiO₂ lattice can inhibit the transformation from anatase to rutile phase at high temperatures, thereby preserving more catalytically active anatase phase TiO₂.

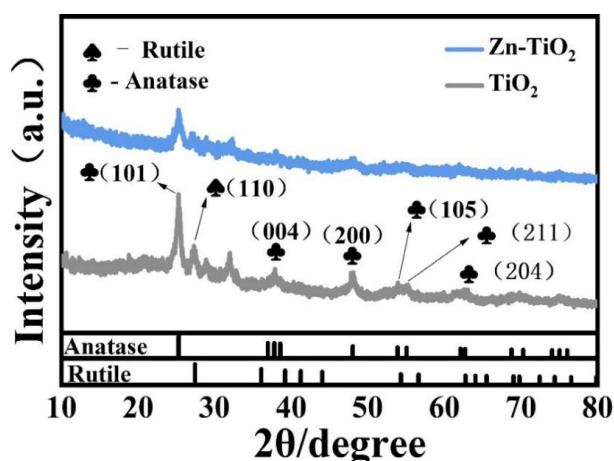


Fig. 2. XRD results of TiO₂, and Zn-TiO₂.

3.3. Photocatalytic degradation of MO

To assess the photocatalytic efficacy of the photocatalysts, the degradation of MO under simulated sunlight illumination was investigated for TiO₂ and Zn-TiO₂, utilizing a UV-visible

spectrophotometer to gauge the photocatalytic activity. As depicted in Fig. 3, changes in the UV-visible spectra were observed over the irradiation period of 0 to 60 minutes (Fig. S3). With increasing visible light exposure time, the concentration of MO decreased. Upon exposure to UV-visible light, the degradation rate of MO was found to be highly efficient by TiO_2 , and Zn-TiO_2 is shown in Fig. 3a, with Zn-TiO_2 exhibiting a higher photocatalytic activity in degrading MO, achieving complete degradation within 30 minutes, while TiO_2 requires 60 minutes to complete the degradation.

To gain deeper insights into the mechanism of photocatalytic dye degradation, we utilized a first-order kinetic model to analyze our experimental findings, as depicted in Fig. 3b. The rate of degradation catalyzed by the photocatalyst is in direct proportion to the concentration of MO. The plot of $\ln(C_0/C_t)$ against time exhibits a linear correlation, pointing to the pseudo-first-order kinetic behavior of MO photocatalytic degradation. By examining the plotted graph, it is possible to calculate the regression coefficients (R^2) and estimate the first-order rate constant (k) based on the kinetic equation $\ln(C_0/C_t) = kt$ [40]. Here, k stands for the rate constant for a first-order reaction. The initial concentration of MO is denoted by C_0 , while C_t represents the concentration of MO at a specific time t , which is expressed in minutes. The kinetic data analysis is summarized in Table 1. It is observed that metal-doped TiO_2 photocatalysts have higher rate constants than pure TiO_2 . Specifically, the Zn-TiO_2 catalyst is found to have a higher rate constant compared to the TiO_2 catalyst.

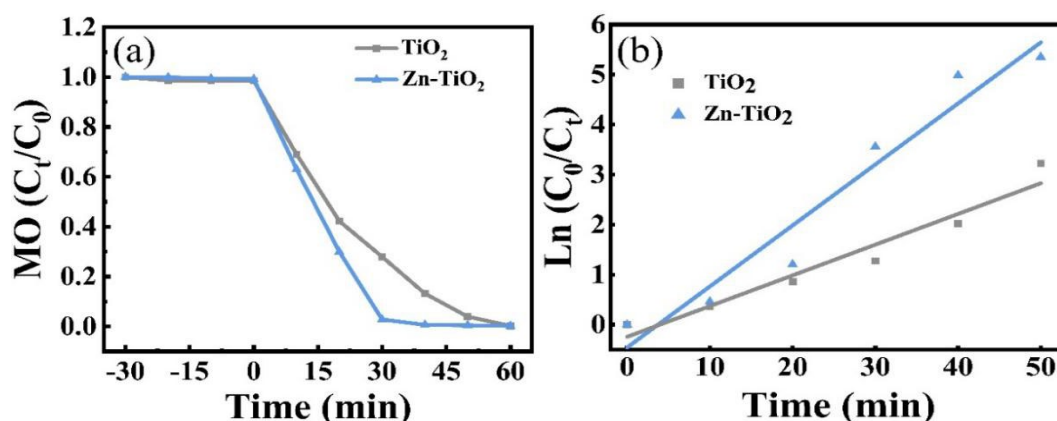


Fig. 3. (a) Photodegradation of MO by different catalysts under UV-vis irradiation. (b) Kinetic study of MO photodegradation by the catalysts.

Table 1. The photocatalytic activity metrics of the photocatalysts.

Photocatalysts	Degradation time (min)	Degradation rate (%)	Degradation completion time (min)	Maximum degradation rate (%)	Apparent reaction rate constant k (min^{-1})	R^2
Pure TiO_2	30	72.15	60	99.74	0.0614	0.9467
Zn-TiO_2	30	97.16	30	97.16	0.1219	0.9477

To delve deeper into evaluating the durability of the synthesized photocatalysts, cyclic degradation tests were conducted. The experimental results are shown in Fig. S4. After 4 cycles, both TiO_2 and Zn-TiO_2 demonstrated good stability and reproducibility. UV-vis spectra (as shown in Fig. S5) indicated their excellent long-term stability and sustainable performance. Results from

cyclic experiments indicated that the photocatalysts maintained high degradation efficiency even after multiple uses without significant degradation trends. Additionally, regeneration or reactivation of the catalyst effectively restored its original catalytic activity, demonstrating excellent stability. Minimal changes in the catalyst's structure and surface characteristics during cyclic use were observed, with no apparent signs of degradation or deactivation.

3.4. Band gap analysis of TiO₂

TiO₂, and Zn-TiO₂ catalysts UV-vis DRS spectra are shown in Fig. 4a. TiO₂ and Zn-TiO₂ catalysts exhibit absorption in the ultraviolet region (200-380 nm). Zn-TiO₂ catalysts demonstrate significantly enhanced absorption between 200-380 nm, with Zn-TiO₂ showing higher absorption. This indicates that Zn doping has a pronounced effect on UV light absorption by TiO₂, enhancing its photocatalytic activity, particularly for Zn-TiO₂. Zn doping likely enhances UV absorption due to its electron energy levels being lower than the conduction band of TiO₂. There is a bandgap blue shift observed between $(\alpha h\nu)^{1/2}$ and $h\nu$ (Fig. 4b). The bandgaps are measured as 3.26 eV for TiO₂, and 3.20 eV for Zn-TiO₂. These results suggest that a reduced bandgap may enhance the photocatalytic degradation of MO, with Zn-TiO₂ exhibiting lower bandgap and higher photocatalytic activity for MO degradation. As shown in Fig. 4c, the horizontal line intersection represents the estimated valence band position (E_{VL}) of the samples. The operational work function (Φ) for the VB-XPS spectrometer is determined to be 4.2 eV. According to equation (1):

$$E_{NHE} = \Phi + E_{VL} - 4.44 \quad (1)$$

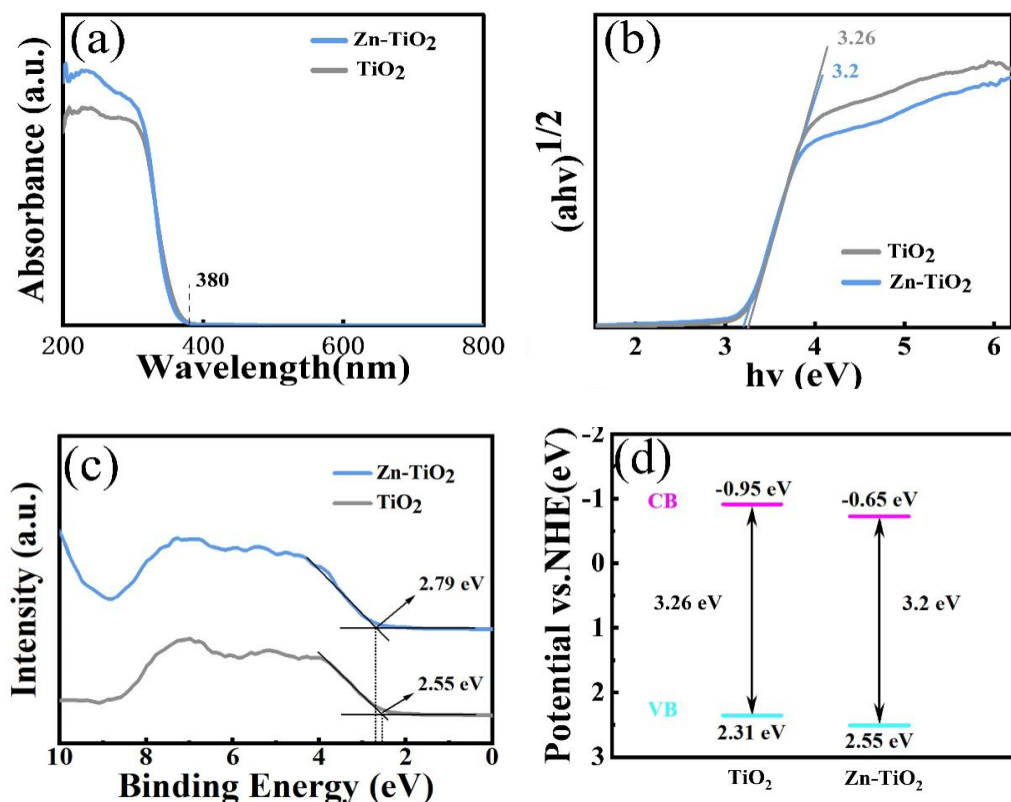


Fig. 4. Mechanism of enhanced photocatalytic performance. (a) UV-Vis spectra of TiO₂, and Zn-TiO₂, (b) Plot of $h\nu$ vs. $(\alpha h\nu)^{1/2}$ showing bandgap characteristics, (c) VB-XPS spectra, and (d) Band structure diagram.

Subsequently, the actual valence band (E_{NHE}) of TiO_2 is calculated as 2.31 eV ($4.2 + 2.55 - 4.44 = 2.31$). Similarly, for Zn-TiO_2 , the valence band is determined to be 2.55 eV [39]. Then, based on the bandgap widths, the energy levels of the conduction bands were determined to be -0.95 eV for TiO_2 , while for Zn-TiO_2 , the value was -0.65 eV (Fig. 4d).

3.5. Study on the photocatalytic mechanism of TiO_2

The PL spectra of all studied photocatalysts are presented. PL emission occurs due to the recombination of charge carriers generated by light absorption (Fig. 5a). Therefore, greater PL intensity suggests a faster rate of charge carrier recombination [41]. TiO_2 exhibits higher emission spectrum, and Zn-TiO_2 exhibits lower. This indicates a suppression of e^- and h^+ recombination rates, thereby enhancing the photocatalytic performance of the catalysts. Among them, Zn-TiO_2 shows lower PL intensity, indicating slower photogenerated charge carrier recombination rate and hence the best photocatalytic performance. Fig. 5b presents the specific surface area bar chart of all studied photocatalysts. TiO_2 exhibits smaller specific surface area, while Zn-TiO_2 shows larger, significantly higher than TiO_2 .

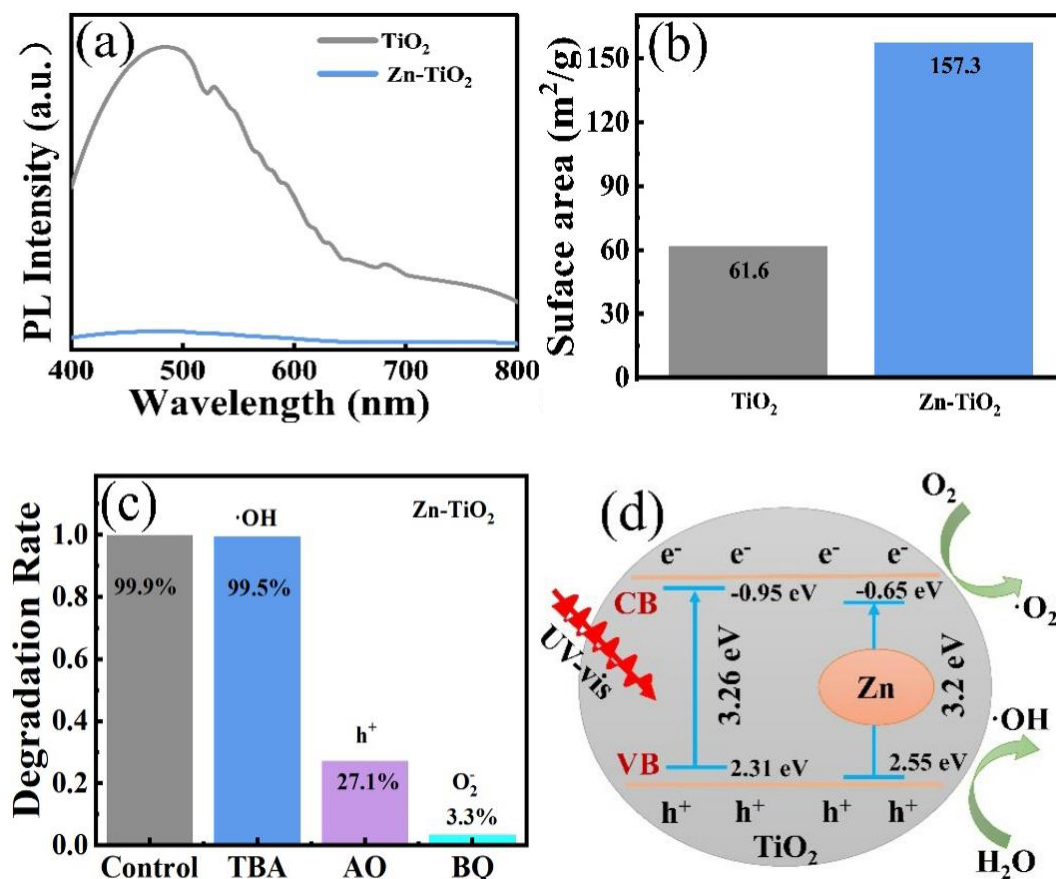


Fig. 5. (a) PL spectra of TiO_2 , and Zn-TiO_2 , and (b) specific surface area bar chart. (c) Degradation efficiency of Zn-TiO_2 under various scavenger conditions. (d) Photocatalytic mechanism diagram of Zn-TiO_2 .

This result demonstrates that Zn doping the catalyst's specific surface area, consistent with the observations in Fig. 1, thereby greatly enhancing the photocatalytic performance of the catalysts. The presented bar graph illustrates the degradation efficiency of Zn-TiO₂ under diverse scavenger treatments, shedding light on the reactive species involved in the photodegradation process of Zn-TiO₂ (Fig.5c). The introduction of TBA, AO, and BQ effectively sequesters hydroxyl radicals ($\cdot\text{OH}$) and superoxide radicals (h^+ , O_2^-), respectively. With the addition of TBA, the catalyst achieved a 99.5% degradation rate for MO, whereas the degradation rates in the presence of AO and BQ were 27.1% and 3.3%, respectively. These findings suggest that TBA has a negligible impact on the photocatalytic activity of the catalyst, in contrast to AO and BQ, which markedly diminish its efficacy. Consequently, superoxide radicals (O_2^- , h^+) are identified as the predominant reactive species and the key determinants affecting the photocatalytic efficiency, as shown in the schematic diagram of the photocatalytic mechanism (Fig. 5d).

4. Conclusion

In summary, this study revealed that the Zn-TiO₂ nanoparticles possess enhanced crystallinity and a significantly larger surface area compared to those synthesized by conventional methods. The unique nano-flower-like morphology, achieved through the use of oxalic acid, further contributes to the superior photocatalytic performance by providing more active sites for the degradation of organic pollutants. SEM results indicated that Zn-TiO₂ adopts a flower-like morphology compared to TiO₂, and exhibits a larger surface area. UV-vis DRS measurements indicated that the band gaps of TiO₂ and Zn-TiO₂ are 3.31 eV and 3.20 eV, respectively. PL spectra showed that TiO₂ had higher emission intensity, followed by lower for Zn-TiO₂ compared to TiO₂.

These results collectively indicate that Zn-TiO₂ exhibits superior photocatalytic activity for MO dye discoloration. UV-vis experimental results demonstrated that TiO₂ exhibited poorer photocatalytic activity, requiring 60 min. In contrast, the enhanced photocatalytic performance of Zn-doped TiO₂ was observed, achieving complete MO degradation in just 30 min, and demonstrating good stability and recyclability. Results from radical trapping studies highlighted the significant role of superoxide radicals O_2^- and h^+ in enhancing photocatalytic activity.

Acknowledgments

This research was funded by Natural Science Foundation of Sichuan Province(2024NSFSC1119), the Research Initiated Project of Chengdu University (2081921109), Open Project of National Engineering Technology Research Centre for Advanced Manufacturing Technology and Equipment of Large Castings and Forgings (Q2304-8).

References

- [1] M. Tahir, S. Tasleem, B. Tahir, International Journal of Hydrogen Energy, **45** (2020) 15985-16038; <https://doi.org/10.1016/j.ijhydene.2020.04.071>

- [2] G. Žerjav, K. Žižek, J. Zavašnik, A. Pintar, *Journal of environmental chemical engineering*, **10** (2022) 107722; <https://doi.org/10.1016/j.jece.2022.107722>
- [3] R. Ranjith, N. Karmegam, M. Alsawalha, X. Hu, K. Jothimani, *Journal of Environmental Management*, **330** (2023) 117132; <https://doi.org/10.1016/j.jenvman.2022.117132>
- [4] Q. Yang, Y.-Y. Mao, Q. Liu, W.-W. He, *Rare Metals*, **42** (2023) 2928-2948; <https://doi.org/10.1007/s12598-023-02309-w>
- [5] T. Bi, Z. Du, S. Chen, H. He, X. Shen, Y. Fu, *Applied Surface Science*, **614** (2023) 156240; <https://doi.org/10.1016/j.apsusc.2022.156240>
- [6] Y. Sun, W. Zhang, Q. Li, H. Liu, X. Wang, *Advanced Sensor and Energy Materials*, (2023) 100069; <https://doi.org/10.1016/j.asems.2023.100069>
- [7] X. Li, C. Li, Y. Xu, Q. Liu, M. Bahri, L. Zhang, N.D. Browning, A.J. Cowan, J. Tang, *Nature Energy*, **8** (2023) 1013-1022; <https://doi.org/10.1038/s41560-023-01317-5>
- [8] R. Hossain, M.A. Uddin, M.A. Khan, *The Journal of Physical Chemistry C*, **127** (2023) 10897-10912; <https://doi.org/10.1021/acs.jpcc.2c06981>
- [9] M. Mersal, A.F. Zedan, G.G. Mohamed, G.K. Hassan, *Scientific Reports*, **13** (2023) 4431; <https://doi.org/10.1038/s41598-023-31625-5>
- [10] L. Chen, M. Arshad, Y. Chuang, T.-B. Nguyen, C.-H. Wu, C.-W. Chen, C.-D. Dong, *Journal of Alloys and Compounds*, **947** (2023) 169577; <https://doi.org/10.1016/j.jallcom.2023.169577>
- [11] Q. Gao, L. Zhou, S. Xu, S. Dai, Q. Zhu, Y. Li, *Environmental Science: Nano*, **10** (2023) 581-594; <https://doi.org/10.1039/D2EN01033J>
- [12] E. Siddhardhan, S. Surender, T. Arumanayagam, *Inorganic Chemistry Communications*, **147** (2023) 110244; <https://doi.org/10.1016/j.inoche.2022.110244>
- [13] E.M. Jubeer, M.A. Manthrammel, P. Subha, M. Shkir, K. Biju, S. AlFaify, *Scientific Reports*, **13** (2023) 16820; <https://doi.org/10.1038/s41598-023-43735-1>
- [14] Y.-J. Zhang, J.-Z. Cheng, Y.-Q. Xing, Z.-R. Tan, G. Liao, S.-Y. Liu, *Materials Science in Semiconductor Processing*, **161** (2023) 107463; <https://doi.org/10.1016/j.mssp.2023.107463>
- [15] S. Higashimoto, Y. Kurikawa, Y. Tanabe, T. Fukushima, A. Harada, M. Murata, Y. Sakata, H. Kobayashi, *Applied Catalysis B: Environmental*, **325** (2023) 122289; <https://doi.org/10.1016/j.apcatb.2022.122289>
- [16] M. Desseigne, V. Madigou, M.-V. Coulet, O. Heintz, V. Chevallier, M. Arab, *Journal of Photochemistry and Photobiology A: Chemistry*, **437** (2023) 114427; <https://doi.org/10.1016/j.jphotochem.2022.114427>
- [17] S. Shabna, S.S.J. Dhas, C. Biju, *Catalysis Communications*, (2023) 106642; <https://doi.org/10.1016/j.catcom.2023.106642>
- [18] F. You, Y. Zhou, D. Li, H. Zhang, D. Gao, X. Ma, R. Hao, J. Liu, *Journal of Colloid and Interface Science*, **629** (2023) 871-877; <https://doi.org/10.1016/j.jcis.2022.09.134>
- [19] C. Liu, M. Zhang, H.-Q. Geng, P. Zhang, Z. Zheng, Y.-L. Zhou, W.-W. He, *Applied Catalysis B: Environmental*, (2021), 120317; <https://doi.org/10.1016/j.apcatb.2021.120317>
- [20] H. Zhou, H. Wang, C. Yue, L. He, H. Li, H. Zhang, S. Yang, T. Ma, *Applied Catalysis B: Environmental*, (2023) 123605; <https://doi.org/10.1016/j.apcatb.2023.123605>
- [21] O.U. Akakuru, Z.M. Iqbal, A. Wu, New York, 2020, pp. 1-66.
- [22] J.A. Rengifo-Herrera, C. Pulgarin, *Chemical Engineering Journal*, (2023) 146875; <https://doi.org/10.1016/j.cej.2023.146875>
- [23] D.R. Eddy, M.D. Permana, L.K. Sakti, G.A.N. Sheha, Solihudin, S. Hidayat, T. Takei, N.

- Kumada, I. Rahayu, *Nanomaterials*, **13** (2023) 704; <https://doi.org/10.3390/nano13040704>
- [24] Y. Zhang, R. Long, *The Journal of Physical Chemistry Letters*, **15** (2024) 6002-6009; <https://doi.org/10.1021/acs.jpcllett.4c01329>
- [25] J. Gao, Y. Chen, J. Shuai, X. Liu, B. Zou, W. Feng, P. Wang, J. Chen, *Digest Journal of Nanomaterials and Biostructures*, **19** (2024) 649-660; <https://doi.org/10.15251/djnb.2024.192.649>
- [26] F. Huang, A. Yan, H. Zhao, *mechanisms and applications*, (2016) 31-80; <https://doi.org/10.5772/63234>
- [27] Y. Sun, Y. Gao, B. Zhao, S. Xu, C. Luo, Q. Zhao, *Materials Research Express*, **7** (2020) 085010; <https://doi.org/10.1088/2053-1591/abaca4>
- [28] P. Akhter, S. Nawaz, I. Shafiq, A. Nazir, S. Shafique, F. Jamil, Y.-K. Park, M. Hussain, *Molecular Catalysis*, **535** (2023) 112896; <https://doi.org/10.1016/j.mcat.2022.112896>
- [29] D.V. Aware, S.S. Jadhav, *Applied Nanoscience*, **6** (2016) 965-972; <https://doi.org/10.1007/s13204-015-0513-8>
- [30] E. Bayan, T. Lupeiko, L. Pustovaya, M. Volkova, V. Butova, A. Guda, *Journal of Alloys and Compounds*, **822** (2020) 153662; <https://doi.org/10.1016/j.jallcom.2020.153662>
- [31] Q. Li, P. Wu, Y. Huang, P. Chen, K. Wu, J. Wu, Y. Luo, L. Wang, S. Yang, Z. Liu, *International Journal of Hydrogen Energy*, **47** (2022) 15641-15654; <https://doi.org/10.1016/j.ijhydene.2022.03.091>
- [32] L. Munguti, F. Dejene, *Nano-Structures & Nano-Objects*, **24** (2020) 100594; <https://doi.org/10.1016/j.nanoso.2020.100594>
- [33] S. Zhao, D.-X. Lin, Y.-X. Wang, *Journal of Nanoelectronics and Optoelectronics*, **16** (2021) 967-973; <https://doi.org/10.1166/jno.2021.3050>
- [34] K. Jiang, J. Zhang, R. Luo, Y. Wan, Z. Liu, J. Chen, *RSC advances*, **11** (2021) 7627-7632; <https://doi.org/10.1039/D0RA09318A>
- [35] V.G. Krishnan, P. Elango, K. Ravikumar, R. Marnadu, O.M. Aldossary, M. Ubaidullah, *New Journal of Chemistry*, **45** (2021) 10488-10495; <https://doi.org/10.1039/D1NJ01079D>
- [36] A. Gunasekaran, A.K. Rajamani, C. Masilamani, I. Chinnappan, U. Ramamoorthy, K. Kaviyarasu, *Catalysts*, **13** (2023) 215; <https://doi.org/10.3390/catal13020215>
- [37] T. Dikici, O. Yılmaz, A. Akalın, S. Demirci, S. Gültekin, S. Yıldırım, M. Yurddaşkal, *Journal of the Australian Ceramic Society*, **58** (2022) 1415-1421; <https://doi.org/10.1007/s41779-022-00712-7>
- [38] M. Carofiglio, S. Barui, V. Cauda, M. Laurenti, *Applied Sciences*, **10** (2020) 5194; <https://doi.org/10.3390/app10155194>
- [39] J. Chen, J. Gao, X. Liu, P. Wang, X. Yu, F. Zhao, Y. Sun, W. Feng, Q. Wang, *Nanomaterials*, **12** (2022) 3019; <https://doi.org/10.3390/nano12173019>
- [40] M.E. Awad, A.M. Farrag, A.A. El-Bindary, M.A. El-Bindary, H.A. Kiwaan, *Applied Organometallic Chemistry*, **37** (2023) e7113; <https://doi.org/10.1002/aoc.7113>
- [41] A. Dhawan, A. Sudhaik, P. Raizada, S. Thakur, T. Ahamad, P. Thakur, P. Singh, C.M. Hussain, *Journal of Industrial and Engineering Chemistry*, **117** (2023) 1-20; <https://doi.org/10.1016/j.jiec.2022.10.001>